Journal Pre-proof

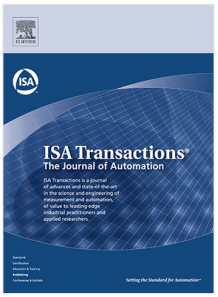

Fuzzy Multi-Regional Fractional PID controller for Pressurized Water nuclear Reactor

Bartosz Puchalski, Tomasz Adam Rutkowski, Kazimierz Duzinkiewicz

PII: S0019-0578(20)30156-7
DOI: https://doi.org/10.1016/j.isatra.2020.04.003
Reference: ISATRA 3552

To appear in: *ISA Transactions*

Received date : 17 April 2019
Revised date : 21 February 2020
Accepted date : 8 April 2020

Please cite this article as: B. Puchalski, T.A. Rutkowski and K. Duzinkiewicz, Fuzzy Multi-Regional Fractional PID controller for Pressurized Water nuclear Reactor. *ISA Transactions* (2020), doi: https://doi.org/10.1016/j.isatra.2020.04.003.

Title: **Fuzzy Multi-Regional Fractional PID controller for Pressurized Water nuclear Reactor**

Authors:

Ph.D. Bartosz Puchalski (bartosz.puchalski@pg.edu.pl);

Ph.D. Tomasz Adam Rutkowski (tomasz.adam.rutkowski@pg.edu.pl);

Ph.D., D.Sc. Kazimierz Duzinkiewicz (kazimierz.duzinkiewicz@pg.edu.pl);

Affiliation: Faculty of Electrical and Control Engineering, Gdańsk University of Technology, G. Narutowicza Street 11/12, 80-233 Gdańsk, Poland

Corresponding author details:

Name: Bartosz Puchalski

Address: Faculty of Electrical and Control Engineering, Gdańsk University of Technology, G. Narutowicza Street 11/12, 80-233 Gdańsk, Poland

Phone: +48 58 347 29 04

E-mail: bartosz.puchalski@pg.edu.pl

Title: **Fuzzy Multi-Regional Fractional PID controller for Pressurized Water nuclear Reactor**

Abstract

The paper presents the methodology for the synthesis of a Fuzzy Multi-Regional Fractional Order PID controller (FMR-FOPID) used to control the average thermal power of a PWR nuclear reactor in the load following mode. The controller utilizes a set of FOPID controllers and the fuzzy logic Takagi-Sugeno reasoning system. The proposed methodology is based on two optimization parts. The first part is devoted to finding the optimal parameters of local FOPID controllers and in the second part, the optimal membership functions of the fuzzy reasoning system are designed. During the controller designing and comparison phase, the two validated nodal models of a nuclear reactor are used, simplified model and extended model respectively. The proposed approach has been verified by computer simulations that confirm its effectiveness.

Keywords: Fractional PID controller; Optimal PID tuning; Fuzzy control; Pressurized Water Reactor (PWR); Takagi-Sugeno (T-S) fuzzy models

1 Introduction

Typically, nuclear power plants operate as the primary energy source in electricity grids. It means that in most cases, the operation of a nuclear power plant is kept constant at full nominal load due to economic and safety reasons. In areas where a noticeable increase in the share of nuclear power plants in the energy balance of the electricity grid is observed, there is a tendency for nuclear power plants to operate in the load-following conditions. In such conditions, the control of the nuclear power plant, and thus the control of its main thermal power generating unit, i.e. the nuclear reactor, should be carried out with the highest possible productivity, which is straightforwardly related with control performance. High control performance can be achieved by improving the existing control algorithms via applying advanced and most modern control technologies. The main objectives of such improved modern control must consider three main goals, which are: 1) plant availability, 2) economic utilization of the nuclear fuel, and 3) operational flexibility for load-following conditions [1]. This paper addresses the third of the above listed tasks.

The energy in the core of a nuclear reactor is produced through a controlled fission reaction of heavy nuclei. This fission is the consequence of neutron absorption by the heavy nucleus, while the probability of neutron absorption is proportional to the neutron flux in the core of the nuclear reactor. Thus, the thermal

power generated in the reactor is directly proportional to the neutron flux in the core. In practice, the neutron flux change is influenced by many processes such as: 1) neutron kinetics, 2) internal feedback effects related to changes in fuel and coolant temperatures, 3) fuel poisoning and burnout, 4) control rod movement, and 5) changes in boron concentration in the primary coolant loop. It should be mentioned here that the movement of the control rods and changes in the concentration of boron in the coolant are treated as controlling effects. The abovementioned processes can be characterised by the time scales with which they occur. Thus, fast processes, which occur in the time range from milliseconds to minutes, include neutron kinetics, feedback effects from changes in fuel and coolant temperatures, and movement of control rods. On the other hand, slow processes, which last from hours to days, include poisoning and burning of fuel, and changes in boron concentration in the coolant.

The objective of nuclear reactor power control is therefore to influence the processes taking place in the nuclear reactor in a controlled way through control effects. Due to a variety of time scales of processes and control effects under consideration, the control problem leads directly to the process of time decomposition of the controlled plant, which in this case is the nuclear reactor. This decomposition, in turn, leads to the design of a multi-level control system that considers such control problem related aspects as safety control, disturbance control, load control, xenon control, core power distribution control, power scheduling, fuel management, system expansion, etc.

Currently, there is a great deal of research related to modern control techniques that allow controlling the main process components within the nuclear power plant which are directly involved in the production of heat and electricity. The most up-to-date and popular solutions make use of modern control techniques, such as: Model Predictive Control [2]–[4], state feedback control [5], [6], robust control [7], fuzzy control [8], [9], sliding mode control [10], gain scheduling [11],fractional order PID control [12], etc. The main motivation of the authors was the use of a combination of well-known and easily implementable in practice methods such as Takagi-Sugeno fuzzy systems [13] and fractional order calculus [14] to design a Fuzzy Multi-Regional Fractional PID controller (FMR-FOPID) which ensures sufficient control performance for the non-linear process (PWR nuclear reactor) with respect to the load variations and external disturbances.

Even though the use of fuzzy logic in control systems dates to the 1960s and 1970s, this idea is still being developed, popular and widely used in the engineering and scientific community. The areas of its application

include: control of hydraulic turbines [15], control of turbo generator systems [16], control of wastewater treatment plant [17], control of robot manipulators [18], biotechnology [19], medical diagnosis systems [20], and many others referred to in [21]–[24].

On the other hand, the first mentions of fractional order calculus appeared at the end of the 17th century, making it a much older technology compared to fuzzy systems. However, the first engineering applications of fractional order calculus did not appear until the 1960s [25]. Like for fuzzy systems, there are many scientific publications related to fractional order calculus in which its applications are described. Up-to-date examples of applications of fractional order calculus are as follows: modelling of nuclear reactor processes [26], [27], network control systems [28], [29], modelling and control of photovoltaic components [30], chaotic control systems [31], finances [32], astronomy [33], [34] and many others referred to in [35].

In this research study, the fractional order calculus is used in the form of the Fractional Order PID (FOPID) controller, which was firstly proposed by Igor Podlubny in 1999 [36]. After introducing the fractional order integration parameter λ and the differentiation parameter μ, the transfer function of the FOPID controller, which is a generalised version of the classic PID controller, can be expressed in the following form [36]

$$G_C(s) = K_p + \frac{K_i}{s^\lambda} + K_d s^\mu, \quad \lambda, \mu > 0, \tag{1}$$

where K_p, K_i, K_d are the proportional, integral, and derivative gains of the controller, respectively, and s is the complex variable.

Compared to the classic PID controller, the FOPID controller in the above form is characterized by two additional degrees of freedom which allow it to be more flexible in shaping the control system closed loop response and thus improving the performance and control quality of the control system under consideration [25], [36].

The second control technique which is used in the research study presented in the paper is related to Takagi-Sugeno fuzzy modelling. The fuzzy implication R defined by Takagi and Sugeno [13] is described as follows

$$\text{R: If } f(x_1 \text{ is } A_1, \dots, x_k \text{ is } A_k) \text{ then } y = g(x_1, \dots, x_k), \tag{2}$$

where y is the variable of consequence whose value is inferred, $x_1, .., x_k$ are the premise variables that appear also in the part of consequence, $A_1, \dots, A_k$ are the fuzzy sets described by membership functions representing

a fuzzy subspace in which the implication R can be applied for reasoning, $f(\cdot)$ is the logical function that connects the propositions in the premise, and $g(\cdot)$ is the function that implies the value of y when $x_1, \ldots, x_k$ satisfies the premise.

These two control techniques were combined by the authors to implement an FMR-FOPID controller that allows the operation of the nuclear reactor within a broad range of work point changes by adapting the controller parameters to changing working conditions. The structure of the multi-regional controller is shown in Figure 1, with the rule base of the fuzzy system described as follows:

$$R_i\text{:If } x_5 \text{ is } A_i, \text{ then } y = u_i(t) \quad \text{for} \quad i = 1, \ldots, 4, \tag{3}$$

where u_i are the local control signals from FOPID controllers designed for operating points of nuclear reactor related to 40%, 60%, 80%, and 100% nominal thermal power P_{TH}. The purpose of the presented multi-regional controller is firstly to improve the quality of control at fixed operating points due to the use of local FOPID controllers which are characterized by greater flexibility in the context of shaping the response of the control system under consideration, and secondly to enable the transition (adaptation) between different operating points of the nuclear reactor through the use of the Takagi-Sugeno fuzzy interference system.

For the purposes of designing the FMR-FOPID controller, the methodology of its synthesis has been prepared, which consists of the following steps: 1) specify the number of local FOPID controllers for the non-linear process control problem, 2) selection of the approximation method for fractional order operators, 3) fine-tune the parameters of the controllers in the local sense, 4) specify the classes of the membership function and tune their shape parameters in the global sense.

This paper is organized as follows. In Section 2 the structure of the nuclear reactor thermal power control system is described, while in Section 3 the proposed FMR-FOPID controller synthesis methodology is presented. The results of verification of the control system with the proposed multi-regional controller are discussed in Section 4, and final conclusions are given in Section 5.

2 Control system structure

The structure of the nuclear reactor thermal power control system which allows a wide range of operating point changes is shown in Figure 2. The presented structure has 3 external inputs and one output. The inputs to

the system are: 1) reference average thermal power $P_{TH,R}$, 2) coolant temperature $T_{C,in}$ at nuclear reactor inlet, and 3) mass flow rate W_C of the coolant through the nuclear reactor. The last two inputs are treated as disturbances in the controlled plant operation. In the control system under consideration, there is also one output corresponding to the average thermal power of the nuclear reactor, labelled as P_{TH}. The internal control system signals are: the control error e, the velocity v_R of control rods, and the reactivity introduced into the core via the movement of control rods, labelled as $\rho_{EXT,R}$. In the presented structure, the FMR-FOPID controller utilizes the control error signal to determine control signals from local FOPID controllers working in parallel and a signal of actually generated average thermal power, also referred to as the leading variable, which is used in the Takagi-Sugeno fuzzy reasoning system as shown in Figure 1.

Parameters of the mathematical models presented in subsections 2.1 and 2.2 are listed in Appendix A.

2.1 Nuclear reactor models

As mentioned before, two nuclear reactor models were used in the research presented in the paper. Structures of the models and descriptions of their parameters and variables which are presented in this chapter have been taken from previous works of the authors [40], [41]. The first model, referred to as the simplified one, was used for synthesising the proposed control system, while the second model, referred to as the extended one, was used for verification and comparison purposes. The unified structure of the nuclear reactor models is shown in Figure 3. The models differ in the number of calculation nodes, which directly affects their complexity and capabilities of reproducing the temperature distribution along the core height. The simplified model consists of a single fuel calculation node and two coolant calculation nodes. These node types are marked yellow and blue, respectively, in Figure 3. On the other hand, the extended model consists of five fuel nodes and ten coolant nodes for calculation purposes. Both models were validated based on simulation studies performed with the 1D nuclear reactor model included in the Apros – nuclear and thermal power process simulation software [37], [38]. The Apros package has been used with successes for various simulation tests and analysis purposes in a series of nuclear power plant projects [38].

The models share a single computational node of neutron kinetics, marked green in Figure 3. The purpose of this node is to calculate the average neutron density. The node is defined by the following differential equations [39]:

$$\frac{d\bar{n}(t)}{dt} = \frac{\rho(t)}{\Lambda}\bar{n}(t) - \frac{\beta}{\Lambda}\bar{n}(t) + \sum_{j=1}^{6}\lambda_j C_j(t), \tag{4}$$

$$\frac{dC_j(t)}{dt} = \frac{\beta_j}{\Lambda}\bar{n}(t) - \lambda_j C_j(t), \quad j = 1, \ldots, 6, \tag{5}$$

where $\bar{n}$ is the averaged neutron density, ρ is the reactivity, $\beta = \sum_{j=6}^{6}\beta_i$ is the total yield of the delayed neutron precursors, Λ is the averaged neutron generation time, λ_j are the delayed neutron precursors decay constants, C_j are the j-th group of the delayed neutron precursors concentrations, β_j are the delayed neutron precursors yields, and t denotes time. The average thermal power P_{TH} generated in the nuclear reactor is directly proportional to the average neutron flux $\bar{\phi}$ or the averaged neutron density $P_{TH}(t) \sim \bar{\phi}(t) \sim \bar{n}(t)$ [37]. Considering this relation, the averaged thermal power generated in the core can be determined as follows [37]

$$P_{TH}(t) = \frac{\bar{n}(t)}{N_N}P_{TH,N}, \tag{6}$$

where $P_{TH,N}$ is the nominal power of the reactor and N_N is the nominal average neutron density at $P_{TH,N}$.

The next computational nodes are related to the determination of temperatures in the nuclear reactor core along its height. The temperature change at fuel nodes is described by the following differential equation

$$\frac{dT_{Fi}(t)}{dt} = D_{Ci}(x)\frac{nf_F P_{TH}(t)}{m_F c_{pF}} - \frac{Ah}{m_F c_{pF}}\left(T_{Fi}(t) - T_{C(2i-1)}(t)\right), \tag{7}$$

where m_F is the fuel mass, c_{pF} is the fuel specific heat capacity, T_{Fi} is the temperature of the fuel at the i-th fuel node, f_F is the fraction of the total power generated in the reactor fuel rods, A is the overall area of the effective heat transfer, h is the average overall heat transfer coefficient, $T_{C(2i-1)}$ is the coolant temperature at the odd coolant node, n denotes the number of the fuel nodes in the model, and D_{Ci} are thermal power distribution coefficients, which are related to the control rod immersion depth x in the reactor core [37], [40].

Temperature changes at coolant nodes are described using the following differential equations. Since there are two computing coolant nodes for each fuel node, they are separated into odd $(2i-1)$ and even nodes $(2i)$

$$\begin{aligned}\frac{dT_{C(2i-1)}(t)}{dt} = D_{Ci}(x)\cdot\frac{n(1-f_F)P_{TH}(t)}{m_C c_{pC}} + \frac{Ah}{m_C c_{pC}}\left(T_{Fi}(t) - T_{C(2i-1)}(t)\right) + \\ -\frac{2nW_C(t)}{m_C}\left(T_{C(2i-1)}(t) - T_{C(2i-2)}(t)\right),\end{aligned} \tag{8}$$

$$\begin{aligned}\frac{dT_{C(2i)}(t)}{dt} = D_{Ci}(x)\cdot\frac{n(1-f_F)P_{TH}(t)}{m_C c_{pC}} + \frac{Ah}{m_C c_{pC}}\left(T_{Fi}(t) - T_{C(2i-1)}(t)\right) + \\ -\frac{2nW_C(t)}{m_C}\left(T_{C(2i)}(t) - T_{C(2i-1)}(t)\right),\end{aligned} \tag{9}$$

where $T_{C(2i)}$ is the coolant temperature at the even coolant node, m_C is the coolant mass, c_{pC} is the coolant specific heat capacity and W_C is the mass flow rate of the coolant within the reactor core. It should be noted here that $i = 1, \dots, n$ is the indexation of calculation nodes [37], [40].

For the above form of the nuclear reactor model, the reactivity feedbacks from the fuel and coolant temperature effects (internal mechanisms) and from the control rod movements (external mechanisms) can be defined as follows [37], [40]

$$\begin{aligned}\rho(t) = \rho_{EXT,R}(t) + \alpha_F \sum_{i=1}^{n}\left[D_{Ci}(x)\cdot\left(T_{Fi}(t) - T_{Fi,N}\right)\right] + \\ +\alpha_C \sum_{i=1}^{n}\left[\frac{1}{2}D_{Ci}(x)\cdot\left(T_{C(2i-1)}(t) - T_{C(2i-1),N}\right) + \right. \\ \left. +\frac{1}{2}D_{Ci}(x)\cdot\left(T_{C(2i)}(t) - T_{C(2i),N}\right)\right],\end{aligned} \tag{10}$$

where $\rho_{EXT,R}$ is the external reactivity deviation from the critical (initial) value, α_F is the reactivity coefficient of the fuel, $T_{Fi,N}$ is the nominal (initial) fuel temperature, α_C is the reactivity coefficient of the coolant and $T_{C(\cdot),N}$ is the nominal (initial) coolant temperature. It should be noted that temperature T_{C0} which results from substituting $i = 1$ to equation (8) is related to the inlet coolant temperature $T_{C0} = T_{C,in}$ and that the sum of all the D_{Ci} coefficients $\sum_{i=1}^{n} D_{Ci} = 1$. It is noteworthy here that the long-term processes, such as burn-out or poisoning of nuclear fuel, are not included in the present unified description of the nuclear reactor model. A more detailed description of the nuclear reactor models used in this study can be found in [37], [40].

2.2 Actuator model

A distinguishing element in the structure of the considered control plant is the actuator, which has the form of the control rod drive. Because of its direct connection with both the controller and the plant, its characteristics cannot be neglected in the synthesis and verification phases of the control system. The model of the actuator was the authors concept inspired by the documentation of the nuclear reactor control rods drive mechanism [41], [42]. In the model of the actuator it was assumed that the reactivity input from control rods is lumped and it is expressed in the form of the ρ_b parameter related to the reactivity worth at the maximum immersion of control rods in the core of the nuclear reactor [37], [43]. With this assumption, in the model of the actuator, the movement of single control rods in the reactor core is not considered. The structure of the developed model of the actuator is presented in Figure 4. The actuator model has one input v_R, which is the control signal from the controller representing the desired speed of the control rods. On the other hand, the actuator model has three outputs, i.e. $\rho_{EXT,R}$, x and $v_{R,sat}$, which represent the reactivity contribution from the

position of the control rods, the position of the control rods, and the signal related to the rod speed, respectively. As can be seen in Figure 4, the control signal from the controller is saturated due to the limit imposed on the maximum speed of the control rods. The position and reactivity signals also have their upper and lower limits related with the assumed extremal positions of the control rods in the reactor core. The minimum and maximum depth of the rods is assumed equal to 30% and 60% of core height, respectively, as seen from the top of the core. Function $f(v_r, x)$ in Fig. 4 is defined as follows

$$f(v_r, x) = \frac{d\rho_{EXT,R}(t)}{dt} = \frac{d\rho_{EXT,R}(x(t))}{dx} \cdot v_R(t) = \frac{\rho_b}{\tilde{H}}\left(1 - \cos\left(\frac{2\pi x(t)}{\tilde{H}}\right)\right) \cdot v_R(t), \tag{11}$$

where ρ_b is the reactivity worth of the control rods at full immersion, and $\tilde{H}$ is the height of the reactor core.

3 FMR-FOPID controller synthesis methodology

The main steps of proposed methodology for the synthesis of a designed FMR-FOPID controller can be presented as follows:

I. Specify the number of local FOPID controllers for the non-linear process control problem.
Comment: This point is directly related to the selection of non-linear process work points where local control is assumed. The number of controllers can be selected e.g. a priori, based on process static characteristics, optimisation or expert knowledge. In the presented work, the number of local controllers was selected a priori based on assumptions presented in subsection 3.1. Nevertheless, the number of local controllers does not influence the overall form of the proposed methodology.

II. Selection of the approximation method for fractional order operators.
Comment: In this step, it is necessary to select the approximation method for operators of fractional order, which are present in FOPID controllers and to determine the necessary parameters that allow proper reconstruction of the dynamics of these operators, which stays with consistency with the dynamics of the plant. In this work, Oustaloup filters were used to approximate the operators of the fractional order. Parameters of these filters were selected in accordance with the dynamics of the plant according to the methodology presented in subsection 3.2.

III. Fine-tune the parameters of the controllers in the local sense.
Comment: Execution of the process of fine-tuning of the parameters of local controllers in agreement with the predefined goals, e.g. regarding the quality of control in a selected work point. In the presented

paper, the process of fine-tuning of the parameters of local controllers was performed optimally, with respect to the chosen integral control quality indexes. This point of the procedure is related to the first part of the optimization task described in subsection 3.3.1.

IV. Specify the classes of the membership function and tune their shape parameters in the global sense.
Comment: In this step, it is necessary to select the membership function classes, which will be used to determine the weights of control signals from individual local controllers based on Takagi-Sugeno reasoning. The number of belonging functions corresponds to the number of local controllers. In this step, it is also necessary to specify the parameters of the shape of the membership functions. In this work, the following classes of membership function were selected: Z, PI, S. The parameters of these functions were selected in an optimal way according to the second part of the optimization task described in subsection 3.3.2.

3.1 Step I – Specify the number of local FOPID controllers

In this research study, the number of local FOPID controllers has been selected a priori on the basis of the following considerations: 1) two of the selected work points, i.e. 100% and 40% P_{TH}, were related to the level of nuclear reactor thermal power corresponding to the nominal operation and to an area of operation which was close to the maximum immersion of the control rods, respectively (this maximum immersion was assumed to be equal to 60% of the height of the reactor core calculated from the top), 2) the remaining two work points, i.e. 80% and 60%, were selected to achieve even distribution and thus to ensure relatively smooth transition between the two outermost work points. Selecting the number of local FOPID controllers was not the focus of the present research.

Hence, the synthesis of the FMR-FOPID controller presented in Introduction, for the PWR nuclear reactor, consists in adjusting parameters of 4 local FOPID controllers and selecting shape parameters for the membership functions used in the fuzzy part (interference system) of the controller. The total of 32 parameters of the controller are available for adjustment. There are 20 parameters related to the local FOPID controllers (5 parameters per each of the 4 local controllers) and 12 parameters related to the membership functions (MF) of the fuzzy part (2 parameters for one Z-type MF, 4 parameters for each of the two PI-type MF, and 2 parameters for one S-type MF). The shapes and parameters of the used membership functions are shown in Figure 5. Due to many controller parameters to be adjusted, a decision was made to use optimization techniques

for this purpose. The developed method of optimization of the controller's parameters is presented in Section 3.3.

3.2 Step II – Determination of the Oustaloup filter parameters

In the present study, fractional order operators in the FOPID controllers are replaced by approximations in the form of Oustaloup filters [44] in order to broaden the applicability of the presented solution. The main disadvantage of numerical procedures calculating fractional-order integrals and derivatives (for instance the Grunwald-Letnikov definition [25]) is that they require infinite memory to store samples of signals which are subjected to the abovementioned operations. The use of the Oustaloup filter overcomes this disadvantage but introduces into the controller synthesis process additional parameters which need to be adjusted. Determining these parameters is necessary for obtaining a satisfactory approximation of fractional operators.

In their paper [44], Alain Oustaloup et al. have presented a filter of fractional order $\alpha \in \mathbb{R}$ in the following form

$$D(s) = \frac{S(s)}{E(s)} = \left(\frac{\omega_u}{\omega_h}\right)^{\alpha} \left(\frac{1+\frac{s}{\omega_b}}{1+\frac{s}{\omega_h}}\right)^{\alpha}, \tag{12}$$

where $E(s)$ is the input signal, $S(s)$ is the output signal, ω_b and ω_h are the transitional frequencies, and $\omega_u = \sqrt{\omega_b \omega_h}$ is the unit gain frequency. The authors also proposed to approximate the above transfer function with a system of integer degree, whose zeroes and poles are recursively distributed on the complex plane according to the following equations [44]

$$D(s) = \lim_{N\to\infty} D_N(s), \text{ where, } D_N(s) = \left(\frac{\omega_u}{\omega_h}\right)^{\alpha} \prod_{k=-N}^{N} \frac{1+s/\omega_k'}{1+s/\omega_k}. \tag{13}$$

where: $-\omega_k'$ is zero of rank k and $-\omega_k$ is pole of rank k.

The recursive form of the filter described by Oustaloup et al. in [44] approximates the fractional order operators in a valid way, under the condition that $\omega_b \omega_h = 1$. In this work a less restrictive version of the Oustaloup filter proposed by Xue et al. in [45] was used, for which the above condition is not needed. This definition is also implemented in Matlab/Simulink FOMCON Toolbox [46] which was used in the presented paper. This filter is described by the following formula

$$D_N(s) = K \prod_{k=-N}^{N} \frac{s+\omega_k'}{s+\omega_k}. \tag{14}$$

Zeros, poles and gain of the integer order filter described by (14) are as follows [45]:

$$\omega_k' = \omega_b \left(\frac{\omega_h}{\omega_b}\right)^{\frac{k+N+\frac{1}{2}(1-\alpha)}{2N+1}}, \tag{15}$$

$$\omega_k = \omega_b \left(\frac{\omega_h}{\omega_b}\right)^{\frac{k+N+\frac{1}{2}(1+\alpha)}{2N+1}}, \tag{16}$$

$$K = \omega_h^{\alpha}, \tag{17}$$

where the parameter N is strictly related to the order of the filter defined as $2N + 1$.

Oustaloup filters are characterized by a very close approximation of theoretical amplitude and phase frequency characteristics of fractional-order integration and differentiation operators, as reported in [47]. Appropriate selection of filter parameters: ω_b, $\omega_h$and N allows very good reproduction of frequency characteristics in the a priori assumed frequency band $[\omega_A,\ \omega_B]$. As reported in [44], to achieve true fractional differentiation and integration over the assumed frequency band $[\omega_A,\ \omega_B]$, two conditions related to transitional frequencies ω_b and ω_h are to be satisfied:

$$w_b \ll w_A \text{ and } \omega_h \gg \omega_B. \tag{18}$$

In this study, the Oustaloup filter frequency band for each FOPID controller was determined using a simplified nuclear reactor model which was linearized at four operating points: 40%, 60%, 80% and 100% P_{TH}. Then, for each obtained linear model, the smallest and the largest real values of zero or pole were determined. The smallest values were used to determine the limit frequency ω_A, while the largest values were used to determine the limit frequency ω_B. The resultant transitional frequencies of the Oustaloup filters for the considered simplified reactor model are given by the following relationships

$$\omega_b = 10^{-2} \cdot \omega_A \text{ and } \omega_h = 10^{2} \cdot \omega_B. \tag{19}$$

The parameter N was selected based on two objectives, which were: 1) satisfactory representation of the theoretical frequency characteristics of fractional operators, 2) relatively low filter order. Taking into account these divergent objectives, it was decided to use N = 7. The results of the calculations are shown in Table I. Figure 6 shows the determined limit frequencies calculated based on the linear simplified nuclear reactor model at different work points.

3.3 Optimization tasks

As mentioned earlier, the multi-regional controller has a total of 32 parameters to be adjusted. With this number of parameters, it was justified to use optimisation techniques to find their optimal values. The structure of the controller (Figure 1) suggested separating the optimization task into two parts. In the first part (step III of controller synthesis methodology), four local FOPID controllers were successively optimized in four independent optimization tasks, while in the second part (step IV of controller synthesis methodology), the parameters responsible for the shape of the membership function in the fuzzy part of the multi-regional controller were optimized in a single optimization task. The overview of the optimization task divided into two parts is shown, in Figure 7. The MADS [48] optimization algorithm was used both in the first and second part of the optimization. The choice of the MADS algorithm was dictated mainly by the nature of the optimization task (black box type optimization). This issue is discussed in detail in Sections 3.3.1 and 3.3.2, where the objective function, defined from the optimizer's point of view, is presented in an implicit manner, and its calculation is performed based on the control system simulation in the Matlab/Simulink computer environment. In such a situation, calculating a priori the form of the objective function gradient is not possible, therefore from the optimizer's point of view, the information about the objective function derivatives can only be approximated, provided that the applied optimization algorithm allows it. The MADS algorithm used in the optimization, along with its most important parameters, is shown in Figure 8.

Due to different nature of each part of the aforementioned optimization, separate trajectories of the thermal power set point were used. The first part of the optimization has a purely local nature; therefore, the trajectory of the thermal power setpoint is constructed in such a way that the extent of deviation from the defined work point is made small. On the other hand, the second part of the optimization has a global nature, so in this case, a trajectory was used which goes in the vicinity of all defined work points and its time horizon is extended. The trajectories of the thermal power set point for the first and second part of the optimization are shown in Figure 9a and 9b, respectively.

3.3.1 Step III - Fine-tune the local FOPID controllers parameters (optimization – part 1)

The optimization task in the first part is defined as follows

$$\min_{\mathbf{x}_{E1,i}} f(\mathbf{x}_{E1,i}), \text{ subject to } \mathbf{x}_{E1,i,lb} \leq \mathbf{x}_{E1,i} \text{ for } i = 1, \dots 4, \tag{20}$$

where $\mathbf{x}_{E1,i} = [K_{Pi}, K_{Ii}, K_{Di}, \lambda_i, \mu_i]$ is the decision variable vector, $f(\mathbf{x}_{E1,i})$ is the objective function to be minimized, and $\mathbf{x}_{E1,i,lb} = [0\ 0\ 0\ 0\ 0]$ is the lower bound vector. In the first part of the optimization, there are no upper bounds. The value of the objective function for each i is evaluated by simulating the operation of the nuclear reactor thermal power control system model, which is illustrated in Figure 10.

In the context of Figure 10, the objective function is defined as follows

$$f(\mathbf{x}_{E1,i}) = J_{E1,i} = \frac{J_{C_{E1}} + \kappa \cdot f_k}{1+\kappa}, \tag{21}$$

where $J_{C_{E1}} = \{J_{ISE}, J_{ITAE}, J_{LQ}\}$ is the exchangeable integral quality performance index, f_k is the penalty function, and $\kappa = 0{,}5$ is the weight of the penalty function. The $v_{R,sat}$ signal marked in Figure 10 with a dashed line is used only in the J_{LQ} integral quality performance index. The integral quality performance indexes J_{ISE}, J_{ITAE}, and J_{LQ} are defined as follows

$$J_{ISE} = \int_0^{t_f} e^2(\tau)d\tau, \quad J_{ITAE} = \int_0^{t_f} \tau|e(\tau)|\,d\tau, \quad J_{LQ} = \int_0^{t_f} \left(Qe^2(\tau) + v_{R,sat}^2(\tau)\right)d\tau, \tag{22}$$

where the weight $Q = 0{,}0625$ has been selected in such a way that the signals e and $v_{R,sat}$ in the performance index J_{LQ} are of the same order of magnitude.

The penalty function has been introduced into the objective function in order to determine the parameters of the local FOPID controllers that would not cause the control signal to significantly exceed the limit values $v_{r,max} = 1{,}9\ cm/s$ and $v_{r,min} = -1{,}9\ cm/s$ associated with the actuator [42]. The values $v_{r,max}$ and $v_{r,min}$ in the actuator correspond, respectively, to the maximum and minimum speed limits for the insertion and withdrawal of the control rods from the reactor core. The block diagram of the penalty function is shown in Figure 11.

The simulation section of the first part of the optimisation task (Figure 10) includes the mechanism for verifying the stability of the linearized control system. The role of this mechanism is to check whether the controller parameters selected by the optimizer do not cause instability of the control system. This mechanism works based on a linearized control system model. If the parameters selected in the optimization process cause instability, such a solution proposal is omitted.

The first part of the optimization task also includes a mechanism which omits the current solution in the simulation part when excessive fluctuations of signals are observed on elements causing discontinuities, in this case the saturation elements in the actuator model (Figure 4). In this case the simulation stops, which results in rejecting the currently considered solution.

3.3.2 Step IV - Fine-tune the fuzzy membership functions parameters (optimization – part 2)

The optimization task in the second part is defined as follows

$$\min_{\mathbf{x}_{E2}} f(\mathbf{x}_{E2}), \text{ subject to } \mathbf{x}_{E2,lb} \leq \mathbf{x}_{E2} \leq \mathbf{x}_{E2,ub} \text{ and } \mathbf{A}_{E2}\mathbf{x}_{E2} \leq \mathbf{b}_{E2}, \tag{23}$$

where $\mathbf{x}_{E2}$ is the decision variable vector, $f(\mathbf{x}_{E2})$ is the objective function to be minimized, $\mathbf{x}_{E2,lb}$ is the lower bound vector, $\mathbf{x}_{E2,ub}$ is the upper bound vector $\mathbf{A}_{E2}$ is the inequality constraint matrix, and $\mathbf{b}_{E2}$ is the inequality constraint vector. Like in the first part of the optimisation, the value of the objective function is evaluated by simulating the operation of the nuclear reactor thermal power control system model developed for this part of the optimization task, as shown in Figure 12.

Unlike the first part of the optimisation, the objective function in the second part does not contain a component related to penalty and stability verification. In this case, the objective function is defined as

$$f(\mathbf{x}_{E2}) = J_{C_{E2}}, \tag{24}$$

where $J_{C_{E2}} = \{J_{ISE}, J_{IAE}, J_{LQR}\}$ is the exchangeable integral quality performance index, and J_{IAE} is defined as:

$$J_{IAE} = \int_0^{t_f} |e(\tau)|\, d\tau. \tag{25}$$

The ITAE criterion used in the first part of the optimisation is replaced with the IAE criterion in the second part, due to a much longer time horizon of the thermal power set-point trajectory used in this part (Fig. 12). A detailed description of the decision variables used in the second part of the optimisation, along with their limit values, is presented in Table II, while the list of inequality constraints is given in Table III.

3.4 Optimization results

This section presents the results of the two-part optimization task formulated for the purpos of steps III and IV of FMR-FOPID controller synthesis methodology. The results are shown in tables which expose the

most important parameters from the optimisation point of view, i.e. the values of the decision variables and the objective function. Individual tables also include starting points from which the optimizer started calculations.

3.4.1 Results of fine-tuning of the local FOPID controllers parameters (optimization – part 1)

This section contains the results of the first part of the optimization task. Table IV presents 4 initial points from which the optimizer started calculations in this part. Points 1 to 3 were selected a priori, while point 4 was selected randomly. Tables V, VI and VII contain the results of the first part of optimization for ISE, ITAE and LQ criteria, respectively. Due to the stochastic nature of the MADS optimization algorithm, a decision was made to run the optimization 5 times for each selected starting point. This resulted in 20 optimization launches for each selected quality criterion in the first part of optimization. For each quality criterion, 4 controllers were optimized (4 work points). Hence, in total, 240 optimiser launches were carried out in the first optimisation part.

3.4.2 Results of fine-tuning of the fuzzy membership functions parameters (optimization – part 2)

This section contains the results of the second part of the optimization task. Like for the first part, 4 initial points were prepared for this part, as shown in Table VIII. All the initialization points, except the first one, have been randomly generated, considering the constraints defined with (23) and presented in Tables II and III. Table IX contains the results of the second part of optimization for ISE, ITAE and LQ criteria, respectively. The shapes of the optimized membership functions for the three integral quality performance indexes used in the second part of the optimization task are shown in Figure 13.

Like in the first part of optimization, in the second part the optimizer was run several times. In this case, the optimizer was run 60 times in total. 5 independent runs were carried out for each of 4 initialization points. Since 3 quality criteria were applied at this stage, this gives 20 runs for each criterion.

4 Verification of simulation tests results

This section presents the results of the performance analysis of the FMR-FOPID controller. This analysis covered three aspects, i.e. the verification, the comparative and the robustness aspect. In the former aspect, the analysis aimed at verifying the efficiency of the FMR-FOPID controller working in the control system in which an extended model of nuclear reactor was used. In the second aspect, the quality of control which was obtained

as a result of operation of the control system with the proposed FMR-FOPID controller was compared to that obtained as a result of the operation of classic equivalents, such as Multi-regional PID controller (FMR-PID), single Fractional Order PID controller (FOPID), and single PID controller (PID). For the last two controllers, it was assumed that their nominal work point is 100% P_{TH}. The third aspect refers to the verification of the robustness of the controllers in the context of rejection of the disturbance quantities related to mass flow W_C and inlet temperature changes $T_{C,in}$ of the coolant.

For each case presented in this section, the quality of control was assessed for controllers whose parameters were obtained as a result of an optimisation task analogous to that presented in Section 3.3. For understandable reasons, the single PID and FOPID controllers were only subjected to the first part of the optimisation task (Sec. 3.3.1). Figure 14 shows the nuclear reactor thermal power control system used for the abovementioned verification and comparison purposes. It also summarises the scenarios within which the controllers have been compared. In the figure, the quantities subject to variation are marked green, while the observable quantities are marked orange.

For verification purposes, two thermal power set point trajectories were selected. The first trajectory has a stepwise character and it is identical with that used in the second part of the optimization (Fig. 9b). The second trajectory, on the other hand, is a fast-alternating sinusoid. The argument behind selecting this trajectory is the wish to periodically force the actuator to work at maximum speed and to check how the compared controllers will perform in such conditions. On the other hand, the robust check of controllers was performed at a constant thermal power signal $P_{TH,R}$, which was set to 100% of the nuclear reactor thermal power and step changes of $T_{C,in}$ and W_C signals. The step changes of $T_{C,in}$ and W_C were set to $\mp$3% and $\mp$10% of the nominal value.

4.1 Stepwise set point trajectory

Figures 15, 16 and 17 show the responses of the control system to stepwise trajectory for the first, second and third verification scenario, respectively. For each of the compared controllers, the figures show the signals of: 1) relative thermal power – $P_{TH}/P_{TH,N}$, 2) speed of control rods – $v_{R,sat}$, 3) position of control rods – x. In each figure, the signals referring to the operation of one of the compared controllers are marked with the same colour. Table X shows the numerical values of integral quality performance indexes for the verification scenarios carried out.

It can be seen in Figure 15 that the response of the control system in which the FMR-FOPID controller is used is characterised by the lowest overshoot and the shortest settling time. The response of this system is not oscillatory in nature, as compared to the responses obtained by the control system with the other compared controllers. Moreover, it can be seen in the control rod velocity plot that the control system working with the FMR-FOPID controller leaves the saturation areas of the actuator most quickly. This directly results in the narrowest span of the control rods in the nuclear reactor core. The results in Figure 15 also show that the control system working with the FMR-FOPID controller is the only system which does not reach the minimum position of the control rods in the reactor core.

Based on Figure 16, it can be concluded that the control system with each of the compared controllers has a similar quality of control. It can also be seen that each controller reaches the vicinity of the operating point in a short time. The control rod position and velocity plots show that the exact value of the thermal power determined by the set point trajectory is reached after a relatively long time, because the speed of the rods does not decrease to zero directly after reaching illusive equilibration of the current thermal power generated by the control object with the setpoint power. On the other hand, the plot of the control rod position has a noticeable slope in the waveform, which occurs after each decay of the transition state. This also confirms slow reaching of the power set point.

It can be seen in Figure 17 that the compared controllers are characterized by similar quality of control, and the control system with the FMR-FOPID controller achieves the lowest settling times during the transition from one work point to the other. This results in increased load of the actuator, as it operates at the maximum possible velocity in longer time periods. Despite this inconvenience, the control system with the FOPID and FMR-FOPID controllers has no integral windup effect. In this comparison, it can also be noticed that the control system with the FMR-PID controller is the only controller that is unable to reach the minimum setpoint level of thermal power. In addition, the response obtained from the control system for each of the compared controllers is inertial in nature.

The values of the integral quality performance index presented in Table X indicate that the control system with controllers based on fractional-order operators is characterized by the best control quality. This conclusion is valid for all verification scenarios considered, particularly the first one. For the first and second verification scenarios, the control system with FMR-FOPID controller is characterized by the lowest value of the integral

quality performance index, while in the third scenario, the control system with the FOPID controller produced the lowest value of the quality index. Relatively, this value is slightly smaller than the quality index identified for the FMR-FPID controller.

4.2 Sinusoidal set point trajectory

Figures 18, 19, and 20 show control system responses to the sinusoidal trajectory for the first, second and third verification scenario, respectively. Like for the stepwise trajectory, for each of the compared controllers, these figures show the signals of: 1) relative thermal power – $P_{TH}/P_{TH,N}$, 2) speed of control rods – $v_{R,sat}$, 3) position of control rods – x. In each figure, the signals referring to the operation of one of the controllers are marked with the same colour. Table XI shows the numerical values of integral quality performance indexes for the verification scenarios carried out using the sinusoidal trajectory.

Figure 18 illustrates the results of the first verification scenario. It shows that when an increased-frequency sinusoidal thermal power setpoint trajectory is used, the control system with PID and FMR-PID controllers is not able to follow the trajectory properly. The use of these controllers causes a large phase shift between the thermal power output reproduced by the control system and the set point thermal power trajectory. Additionally, the response amplitude of the control system with these controllers varies, while the control system with FOPID and FMR-FOPID controllers reproduces the setpoint power trajectory with a small phase shift and almost invariable amplitude. Moreover, as can be seen in the control rod velocity and position plots, the actuator operates with very high load. The saw-like shape of the control rod position plots indicates that the actuator is not able to move the rods faster. The advantage of FOPID and FMR-FOPID controllers can be seen here, mainly as their faster reaction to setpoint trajectory changes, which manifests itself by almost immediate departure of the control system from actuator saturation areas, without any integral windup effect.

It can be concluded from Figure 19 that the optimisation of controller settings according to ITAE/IAE integral performance indexes leads to the situation that the control system with different types of controllers works in an almost identical way. The same situation was observed for the step trajectory (Figure 16). The control rod velocity plots for a control system making use of the FMR-PID controller reveal visible spikes, caused by imprecise switching of control signals in the fuzzy part of the controller, which is mainly related to the shape parameters of the used membership functions.

Figure 20 shows a slight phase shift between the thermal power output reproduced by the control system and the set point thermal power trajectory. Its presence is recorded for all the controllers used. However, in the context of control quality, the smallest phase shift is observed for the control system with FMR-FOPID controllers. It can also be seen that the speed control signals from all the controllers are very similar in this case.

It can be concluded from the summary of integral performance indexes given in Table XI that a control system using FOPID and FMR-FOPID controllers has the best control quality for a sinusoidal thermal power setpoint trajectory. As for the case of stepwise trajectory, it was the control system with the FOPID controller which obtained the lowest value of the quality index in the third verification scenario.

4.3 Stepwise coolant temperature changes

Figures 21, 22 and 23 show the responses of the control system to the first, second and third disturbance rejection scenario related to stepwise coolant temperature changes. In this case, the figures show: 1) the variation of the disturbance quantity – $T_{C,in}$, 2) the relative thermal power of the nuclear reactor – $P_{TH}/P_{TH,N}$, 3) velocity of the control rods – $v_{R,sat}$ for each of the compared controllers. Table *XII* summarizes numerical values of integral quality performance indexes for robustness tests.

Differences between FMR-PID and FMR-FOPID controllers can be seen on the plots showing the results for the rejection of coolant temperature disturbances. In this case, the local PID and FOPID controllers tuned for the 100% thermal power of a nuclear reactor match their multi-regional equivalents. The figures show that the FMR-FOPID controller rejects the disturbance associated with the change of coolant temperature more effectively than the FMR-PID controller, except for the situation shown in Figure 22, where each of the controllers works similarly. Similar behaviour for IAE criterion has been observed before for scenarios with step power changes and sinusoidal power changes.

Numerical values of integral quality indexes presented in table *XII* also confirm the advantage of the fractional order controllers over the classical ones in the context of control quality.

In this part, the figures for mass flow changes of the coolant were omitted from presentation because the control system with the controllers investigated in the paper turned out to be very insensitive to changes of this disturbance quantity within the assumed limits.

5 Conclusions

The paper presents the synthesis of the Fuzzy Multi-Regional Fractional PID controller (FMR-FPID) for controlling the average thermal power of a PWR nuclear reactor in the load following mode. The authors propose and describe a two-stage optimization procedure to find optimal parameters for the FMR-FOPID controller. At the first stage, the parameters of local FOPID controllers are found by solving independent optimization tasks. Then, at the second stage, the parameters responsible for the shape of the membership function in the fuzzy part of the multi-regional controller are found by solving an appropriately defined optimization task. The number of local FOPID controllers was set a priori and is not the focus of the paper. At both stages, the optimization procedure makes use of the Mesh Adaptive Direct Search (MADS) algorithm for constrained minimization and the simplified nuclear reactor model. While in the FMR-FOPID controller verification phase, an extended model of a nuclear reactor is used. Both models were previously validated with reference model – 1D nuclear reactor model included in the nuclear and thermal power process simulation package Apros [37], [38].

The simulation results demonstrate the reliability of proposed FMR-FOPID controller and prove that the methodology of synthesis proposed in the paper is adequate. Comparison with FMR-PID controller, single FOPID controller, and single PID controller showed the superiority of the proposed FMR-FOPID controller by better or comparable values of overall quality control indicators defined, for comparison purposes, between specific simulation scenarios performed during the verification process including robustness verification scenarios. Additionally, simulation results showed that the proposed FMR-FOPID controller may be used for designing of effective controllers which allows to control the complex, non-linear process within a wide range of working point changes.

Acknowledgements

The research work was done under grant Polish MNiSW 8902/E-359/M/2018: Young Researcher Support Program. The authors wish to express their thanks for support.

References

[1] B. Frogner and H. Rao, "Control of nuclear power plants," *IEEE Trans. Automat. Contr.*, vol. 23, no. 3, pp. 405–417, Jun. 1978.

[2] H. Eliasi, M. B. Menhaj, and H. Davilu, "Robust nonlinear model predictive control for nuclear power plants in load following operations with bounded xenon oscillations," *Nucl. Eng. Des.*, vol. 241, no. 2, pp. 533–543, Feb. 2011.

[3] P. Sokólski, T. A. Rutkowski, and K. Duzinkiewicz, "The QDMC Model Predictive Controller for the Nuclear Power Plant Steam Turbine Control," Springer, Cham, 2017, pp. 241–250.

[4] P. Sokolski, T. A. Rutkowski, and K. Duzinkiewicz, "The distributed model predictive controller for the nuclear power plant turbo-generator set," in *2017 22nd International Conference on Methods and Models in Automation and Robotics (MMAR)*, 2017, pp. 682–687.

[5] M. Das *et al.*, "Network Control System Applied to a Large Pressurized Heavy Water Reactor," *IEEE Trans. Nucl. Sci.*, vol. 53, no. 5, pp. 2948–2956, Oct. 2006.

[6] M. Czapliński, P. Sokólski, K. Duzinkiewicz, R. Piotrowski, and T. Rutkowski, "Comparison of state feedback and PID control of pressurizer water level in nuclear power plant," *degruyter.com*.

[7] K. Torabi, O. Safarzadeh, and A. Rahimi-Moghaddam, "Robust Control of the PWR Core Power Using Quantitative Feedback Theory," *IEEE Trans. Nucl. Sci.*, vol. 58, no. 1, pp. 258–266, Feb. 2011.

[8] R. Coban, "A fuzzy controller design for nuclear research reactors using the particle swarm optimization algorithm," *Nucl. Eng. Des.*, vol. 241, no. 5, pp. 1899–1908, May 2011.

[9] B. Puchalski, K. Duzinkiewicz, and T. Rutkowski, "Multi-region fuzzy logic controller with local PID controllers for U-tube steam generator in nuclear power plant," *Arch. Control Sci.*, vol. 25, no. 4, pp. 429–444, 2015.

[10] G. R. Ansarifar and H. R. Akhavan, "Sliding mode control design for a PWR nuclear reactor using sliding mode observer during load following operation," *Ann. Nucl. Energy*, vol. 75, pp. 611–619, Jan. 2015.

[11] P. Sokólski, T. A. Rutkowski, and K. Duzinkiewicz, "The excitation controller with gain scheduling mechanism for synchronous generator control," in *2015 20th International Conference on Methods and Models in Automation and Robotics (MMAR)*, 2015, pp. 23–28.

[12] B. Puchalski, T. A. Rutkowski, and K. Duzinkiewicz, "Implementation of the FOPID Algorithm in the PLC Controller - PWR Thermal Power Control Case Study," in *2018 23rd International Conference on Methods & Models in Automation & Robotics (MMAR)*, 2018, pp. 229–234.

[13] T. Takagi and M. Sugeno, "Fuzzy identification of systems and its applications to modeling and control," *IEEE Trans. Syst. Man. Cybern.*, vol. SMC-15, no. 1, pp. 116–132, Jan. 1985.

[14] K. B. Oldham and J. Spanier, *The fractional calculus: theory and applications of differentiation and integration to arbitrary order*. Dover Publications, 2006.

[15] C. Li, Y. Mao, J. Zhou, N. Zhang, and X. An, "Design of a fuzzy-PID controller for a nonlinear hydraulic turbine governing system by using a novel gravitational search algorithm based on Cauchy mutation and mass weighting," *Appl. Soft Comput.*, vol. 52, pp. 290–305, Mar. 2017.

[16] P. Sokólski, K. Kulkowski, A. Kobylarz, K. Duzinkiewicz, T. A. Rutkowski, and M. Grochowski, "Advanced control structures of turbo generator system of nuclear power plant," *yadda.icm.edu.pl*.

[17] M. Grochowski and T. A. Rutkowski, "Supervised model predictive control of wastewater treatment plant," in *2016 21st International Conference on Methods and Models in Automation and Robotics (MMAR)*, 2016, pp. 613–618.

[18] Byung Kook Yoo and Woon Chul Ham, "Adaptive control of robot manipulator using fuzzy compensator," *IEEE Trans. Fuzzy Syst.*, vol. 8, no. 2, pp. 186–199, Apr. 2000.

[19] J.-I. Horiuchi, "Fuzzy modeling and control of biological processes," *J. Biosci. Bioeng.*, vol. 94, no. 6, pp. 574–578, Dec. 2002.

[20] K.-P. Adlassnig, "Fuzzy Set Theory in Medical Diagnosis," *IEEE Trans. Syst. Man. Cybern.*, vol. 16, no. 2, pp. 260–265, 1986.

[21] G. Feng, "A Survey on Analysis and Design of Model-Based Fuzzy Control Systems," *IEEE Trans. Fuzzy Syst.*, vol. 14, no. 5, pp. 676–697, Oct. 2006.

[22] R. Babuška and H. B. Verbruggen, "An overview of fuzzy modeling for control," *Control Eng. Pract.*, vol. 4, no. 11, pp. 1593–1606, Nov. 1996.

[23] P. Sokólski, T. A. Rutkowski, and K. Duzinkiewicz, "Simplified, multiregional fuzzy model of a nuclear power plant steam turbine," in *2016 21st International Conference on Methods and Models in Automation and Robotics (MMAR)*, 2016, pp. 379–384.

[24] B. Puchalski, T. Rutkowski, J. Tarnawski, and K. Duzinkiewicz, "Comparison of tuning procedures based on evolutionary algorithm for multi-region fuzzy-logi PID controller for non-linear plant," in *2015 20th International Conference on Methods and Models in Automation and Robotics (MMAR)*, 2015, pp. 897–902.

[25] D. Xue, *Fractional-order control systems : fundamentals and numerical implementations*. De Gruyter, 2017.

[26] T. K. Nowak, K. Duzinkiewicz, and R. Piotrowski, "Numerical Solution of Fractional Neutron Point Kinetics Model in Nuclear Reactor," *Arch. Control Sci.*, vol. 24, no. 2, pp. 129–154, Jan. 2014.

[27] T. K. Nowak, K. Duzinkiewicz, and R. Piotrowski, "Numerical solution analysis of fractional point kinetics and heat exchange in nuclear reactor," *Nucl. Eng. Des.*, vol. 281, pp. 121–130, Jan. 2015.

[28] I. Pan, S. Das, and A. Gupta, "Handling packet dropouts and random delays for unstable delayed processes in NCS by optimal tuning of PIλDμ controllers with evolutionary algorithms," *ISA Trans.*, vol. 50, no. 4, pp. 557–572, Oct. 2011.

[29] S. Das, I. Pan, and S. Das, "Fractional order fuzzy control of nuclear reactor power with thermal-hydraulic effects in the presence of random network induced delay and sensor noise having long range dependence," *Energy Convers. Manag.*, vol. 68, pp. 200–218, Apr. 2013.

[30] C.-H. Lin, C.-H. Huang, Y.-C. Du, and J.-L. Chen, "Maximum photovoltaic power tracking for the PV array using the fractional-order incremental conductance method," *Appl. Energy*, vol. 88, no. 12, pp. 4840–4847, Dec. 2011.

[31] W. M. Ahmad and J. C. Sprott, "Chaos in fractional-order autonomous nonlinear systems," *Chaos, Solitons & Fractals*, vol. 16, no. 2, pp. 339–351, Mar. 2003.

[32] W.-C. Chen, "Nonlinear dynamics and chaos in a fractional-order financial system," *Chaos, Solitons & Fractals*, vol. 36, no. 5, pp. 1305–1314, Jun. 2008.

[33] A. C. Sparavigna and P. Milligan, "Using fractional differentiation in astronomy," Oct. 2009.

[34] R. Marazzato and A. C. Sparavigna, "Astronomical image processing based on fractional calculus: the AstroFracTool," Oct. 2009.

[35] J. T. Machado, V. Kiryakova, and F. Mainardi, "Recent history of fractional calculus," *Commun. Nonlinear Sci. Numer. Simul.*, vol. 16, no. 3, pp. 1140–1153, Mar. 2011.

[36] I. Podlubny, "Fractional-order systems and PI/sup /spl lambda//D/sup /spl mu//-controllers," *IEEE Trans. Automat. Contr.*, vol. 44, no. 1, pp. 208–214, Jan. 1999.

[37] B. Puchalski, T. A. Rutkowski, and K. Duzinkiewicz, "Nodal models of Pressurized Water Reactor core for control purposes – A comparison study," *Nucl. Eng. Des.*, vol. 322, pp. 444–463, Oct. 2017.

[38] "Apros - Dynamic Process Simulation Software for Nuclear and Thermal Power Plant Applications."

[Online]. Available: http://www.apros.fi/en. [Accessed: 28-Oct-2019].

[39] J. Duderstadt and L. Hamilton, "Nuclear reactor analysis," 1976.

[40] B. Puchalski, T. A. Rutkowski, and K. Duzinkiewicz, "Multi-nodal PWR reactor model — Methodology proposition for power distribution coefficients calculation," in *2016 21st International Conference on Methods and Models in Automation and Robotics (MMAR)*, 2016, pp. 385–390.

[41] "Westinghouse Technology Systems Manual Section 2.1 Reactor Physics Review." [Online]. Available: https://www.nrc.gov/docs/ML1122/ML11223A207.pdf. [Accessed: 28-Oct-2019].

[42] D. Testa, Ed., *The Westinghouse Pressurized Water Reactor Nuclear Power Plant*. Westinghouse Electric Corporation, Water Reactor Division, 1984.

[43] E. E. Lewis, *Fundamentals of Nuclear Reactor Physics*. Elsevier, 2008.

[44] A. Oustaloup, F. Levron, B. Mathieu, and F. M. Nanot, "Frequency-band complex noninteger differentiator: Characterization and synthesis," *IEEE Trans. Circuits Syst. I Fundam. Theory Appl.*, vol. 47, no. 1, pp. 25–39, 2000.

[45] D. Xue, Y. Chen, and D. P. Atherton, *Linear Feedback Control: Analysis and Design with MATLAB*. SIAM, 2007.

[46] A. Tepljakov, E. Petlenkov, and J. Belikov, "FOMCON: Fractional-order modeling and control toolbox for MATLAB," *Proc. 18th Int. Conf. Mix. Des. Integr. Circuits Syst. - Mix. 2011*, no. 4, pp. 684–689, 2011.

[47] C. A. Monje, Y. Chen, B. M. Vinagre, D. Xue, and V. Feliu, *Fractional-order Systems and Controls*. London: Springer London, 2010.

[48] C. Audet and J. E. Dennis, "Mesh Adaptive Direct Search Algorithms for Constrained Optimization," *SIAM J. Optim.*, vol. 17, no. 1, pp. 188–217, Jan. 2006.

Tables

Table I Parameters of Oustaloup filters for different work points of nuclear reactor

Work point	40% P_{TH}	60% P_{TH}	80% P_{TH}	100% P_{TH}
Limit frequency ω_A [rad/s]	0,012016	0,012155	0,01222	0,012258
Transitional frequency ω_b [rad/s]	0,00012016	0,00012155	0,0001222	0,00012258
Limit frequency ω_B [rad/s]	363,45	363,36	363,26	363,16
Transitional frequency ω_h [rad/s]	36345	36336	36326	36316
Filter order for $N = 7$		15		

Table II Description of decision variables used in the second part of optimisation and their bounds

Decision variable $\mathbf{x}_{E2}$	Membership function class	Description of membership function parameter	Work point $P_{TH,N}$	Lower limit value $\mathbf{x}_{E2,lb}$	Upper limit value $\mathbf{x}_{E2,ub}$
$x_{E2,1}$	$Z_{\tilde{A}_{I5,1}}$	Maximum of descent slope $a_{\tilde{A}_{I5,1}}$	40%	0,3	0,5
$x_{E2,2}$		Minimum of descent slope $b_{\tilde{A}_{I5,1}}$	40%	0,3	1
$x_{E2,3}$	$\Pi_{\tilde{A}_{I5,2}}$	Minimum of ascending slope $a_{\tilde{A}_{I5,2}}$	60%	0,3	1
$x_{E2,4}$		Maximum of ascending slope $b_{\tilde{A}_{I5,2}}$	60%	0,5	1
$x_{E2,5}$		Maximum of descent slope $c_{\tilde{A}_{I5,2}}$	60%	0,3	0,7
$x_{E2,6}$		Minimum of descent slope $d_{\tilde{A}_{I5,2}}$	60%	0,3	1
$x_{E2,7}$	$\Pi_{\tilde{A}_{I5,3}}$	Minimum of ascending slope $a_{\tilde{A}_{I5,3}}$	80%	0,3	1
$x_{E2,8}$		Maximum of ascending slope $b_{\tilde{A}_{I5,3}}$	80%	0,7	1
$x_{E2,9}$		Maximum of descent slope $c_{\tilde{A}_{I5,3}}$	80%	0,3	0,9
$x_{E2,10}$		Minimum of descent slope $d_{\tilde{A}_{I5,3}}$	80%	0,3	1
$x_{E2,11}$	$S_{\tilde{A}_{I5,4}}$	Minimum of ascending slope $a_{\tilde{A}_{I5,4}}$	100%	0,3	1
$x_{E2,12}$		Maximum of ascending slope $b_{\tilde{A}_{I5,4}}$	100%	0,9	1

Table III List of inequality constraints for the second part of optimization

Membership function		
Shape	Core	Boundary endings
$x_{E2,1} \leq x_{E2,2}$	$x_{E2,2} \leq x_{E2,4}$	$x_{E2,3} - x_{E2,2} \leq -0{,}02$
$x_{E2,3} \leq x_{E2,4}$	$x_{E2,1} \leq x_{E2,3}$	$x_{E2,7} - x_{E2,6} \leq -0{,}02$
$x_{E2,4} \leq x_{E2,5}$	$x_{E2,5} \leq x_{E2,7}$	$x_{E2,11} - x_{E2,10} \leq -0{,}02$
$x_{E2,5} \leq x_{E2,6}$	$x_{E2,6} \leq x_{E2,8}$	
$x_{E2,7} \leq x_{E2,8}$	$x_{E2,9} \leq x_{E2,11}$	
$x_{E2,8} \leq x_{E2,9}$	$x_{E2,10} \leq x_{E2,12}$	
$x_{E2,9} \leq x_{E2,10}$		
$x_{E2,11} \leq x_{E2,12}$		

Table IV Initial points of the first part of optimisation

Initial point	1	2	3	4
K_P	0,01	0,1	1	0,8304
K_I	0,01	0,1	1	0,6736
K_D	0,01	0,1	1	0,1395
λ	0,01	0,1	1	0,7431
μ	0,01	0,1	1	0,3922

Table V Results of the first part of optimisation for the ISE integral quality performance index

ISE integral quality performance index				
Work point	40% $P_{TH,N}$	60% $P_{TH,N}$	80% $P_{TH,N}$	100% $P_{TH,N}$
Initial point	2	2	4	4
K_P	0,0000	0,0961	0,0764	0,0804
K_I	0,1797	0,1033	0,1020	0,1111
K_D	0,0000	0,0228	0,0561	0,0272
λ	0,2031	0,4931	0,6273	0,4931
μ	0,9141	0,3922	0,2016	0,2516
Objective function value	0,0273	0,0180	0,0163	0,0212

Table VI Results of the first part of optimisation for the ITAE integral quality performance index

ITAE integral quality performance index				
Work point	40% $P_{TH,N}$	60% $P_{TH,N}$	80% $P_{TH,N}$	100% $P_{TH,N}$
Initial point	1	1	1	3
K_P	0,0000	0,1094	0,1436	0,1176
K_I	2,9375	3,3594	2,9053	0,7777
K_D	1,5000	2,0063	3,0156	4,6313
λ	0,0000	0,0000	0,0000	0,0023
μ	0,0156	0,0042	0,0000	0,0006
Objective function value	19,9975	14,7171	13,9764	19,7023

Table VII Results of the first part of optimisation for the LQ integral quality performance index

LQ integral quality performance index				
Work point	40% $P_{TH,N}$	60% $P_{TH,N}$	80% $P_{TH,N}$	100% $P_{TH,N}$
Initial point	1	1	1	1
K_P	0,0000	0,0256	0,0134	0,0083
K_I	0,0479	0,1663	0,2031	0,1789
K_D	0,1563	0,0207	0,0000	0,0287
λ	0,4072	0,1428	0,1096	0,1168
μ	0,0220	0,0139	1,0000	0,0122
Objective function value	0,0036	0,0028	0,0028	0,0038

Table VIII Initial points of the second part of optimisation

Decision variable $\mathbf{x}_{E2}$	Membership function class	Initial point			
		1	2	3	4
$x_{E2,1}$	$Z_{\tilde{A}_{I5,1}}$	0,4500	0,3172	0,3000	0,3000
$x_{E2,2}$		0,5500	0,4759	0,4729	0,3200
$x_{E2,3}$	$\Pi_{\tilde{A}_{I5,2}}$	0,4500	0,3923	0,3893	0,3000
$x_{E2,4}$		0,5500	0,5000	0,5000	0,5000
$x_{E2,5}$		0,6500	0,5000	0,5526	0,5000
$x_{E2,6}$		0,7500	0,6689	0,6661	0,5200
$x_{E2,7}$	$\Pi_{\tilde{A}_{I5,3}}$	0,6500	0,5000	0,5970	0,5000
$x_{E2,8}$		0,7500	0,7176	0,7000	0,7000
$x_{E2,9}$		0,8500	0,7419	0,7000	0,7000
$x_{E2,10}$		0,4500	0,3172	0,3000	0,3000
$x_{E2,11}$	$S_{\tilde{A}_{I5,4}}$	0,5500	0,4759	0,4729	0,3200
$x_{E2,12}$		0,4500	0,3923	0,3893	0,3000

Table IX Results of the second part of optimisation

Decision variable $\mathbf{x}_{E2}$	Membership function class	Integral quality performance index		
		ISE	IAE	LQ
$x_{E2,1}$	$Z_{\tilde{A}_{I5,1}}$	0,3753	0,3050	0,3007
$x_{E2,2}$		0,5666	0,3556	0,3311
$x_{E2,3}$	$\Pi_{\tilde{A}_{I5,2}}$	0,5417	0,3063	0,3019
$x_{E2,4}$		0,5701	0,5033	0,5195
$x_{E2,5}$		0,5719	0,5371	0,5258
$x_{E2,6}$		0,7563	0,6309	0,5585
$x_{E2,7}$	$\Pi_{\tilde{A}_{I5,3}}$	0,7373	0,5496	0,5395
$x_{E2,8}$		0,7625	0,7238	0,7000
$x_{E2,9}$		0,7636	0,7316	0,7253
$x_{E2,10}$		0,8597	0,9393	0,7650
$x_{E2,11}$	$S_{\tilde{A}_{I5,4}}$	0,7681	0,8497	0,7399
$x_{E2,12}$		0,9090	0,9388	0,9314
Objective function value		1,4846	10,6763	0,1247
Best solution at initial point number		1	3	3

Table X Numerical values of integral quality performance indexes for three stepwise trajectory verification scenarios, the best values are marked bold

Verification scenario	Evaluation criterion	Controller			
		PID	FOPID	FMR-PID	FMR-FOPID
First	ISE	2,2735	1,4508	2,4069	**1,3796**
Second	IAE	9,6601	9,6574	9,6578	**9,6540**
Third	LQ	0,11512	**0,11354**	0,13953	0,11384

Table XI Numerical values of integral quality performance indexes for sinusoidal trajectory verification scenarios, the best values are marked bold

Verification scenario	Evaluation criterion	Controller			
		PID	FOPID	FMR-PID	FMR-FOPID
First	ISE	103,5991	16,2544	112,5475	**3,9041**
Second	IAE	6,3585	6,3090	6,2933	**6,2658**
Third	LQ	0,42493	**0,35991**	0,47782	0,36413

Table XII Numerical values of integral quality performance indexes for stepwise coolant temperature changes robustness check scenarios, the best values are marked bold

Verification scenario	Evaluation criterion	Controller			
		PID	FOPID	FMR-PID	FMR-FOPID
First	ISE	3,7986	**1,8583**	3,7987	**1,8583**
Second	IAE	7,5100	**7,5088**	7,5095	**7,5088**
Third	LQ	0,12256	**0,12717**	0,12256	0,12718

Figures

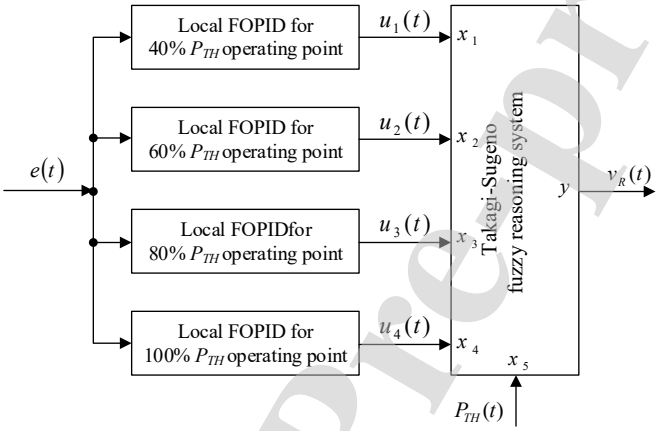

Figure 1 Multi-region fractional fuzzy logic controller structure

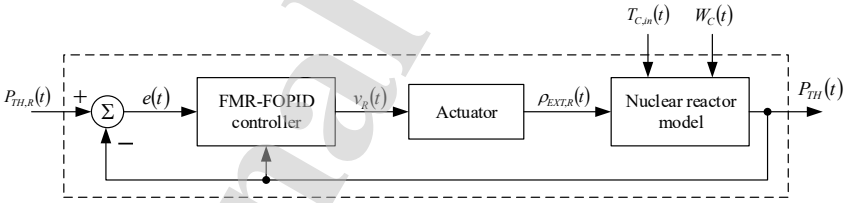

Figure 2 Structure of the reactor thermal power control system under consideration

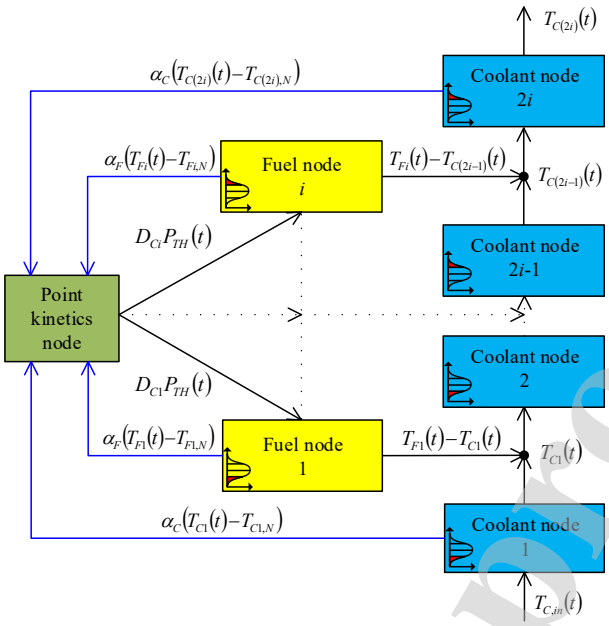

Figure 3 Unified nodal structure of nuclear reactor models

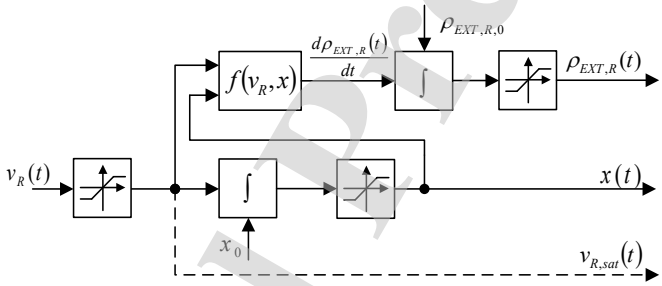

Figure 4 Structure of the actuator model

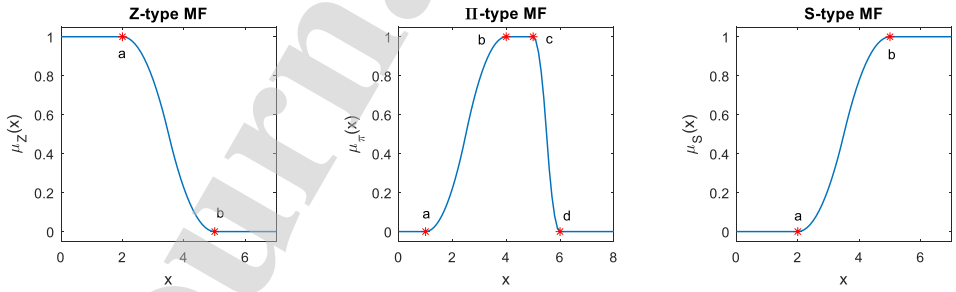

Figure 5 Exemplary membership function shapes that have been used in the fuzzy part of the multi-region controller

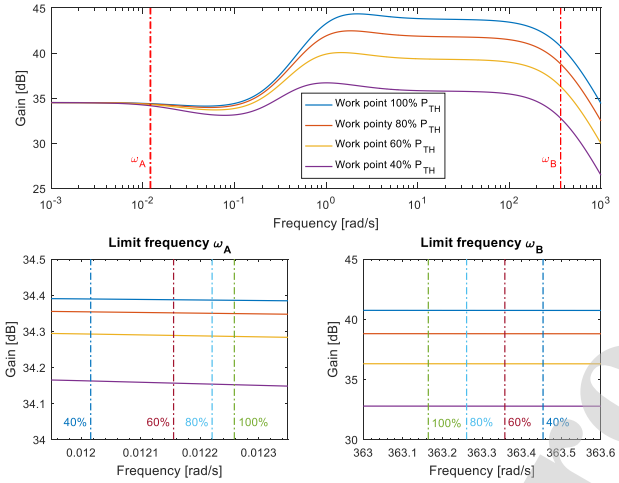

Figure 6 Limit frequencies of the linear simplified nuclear reactor model at different work points

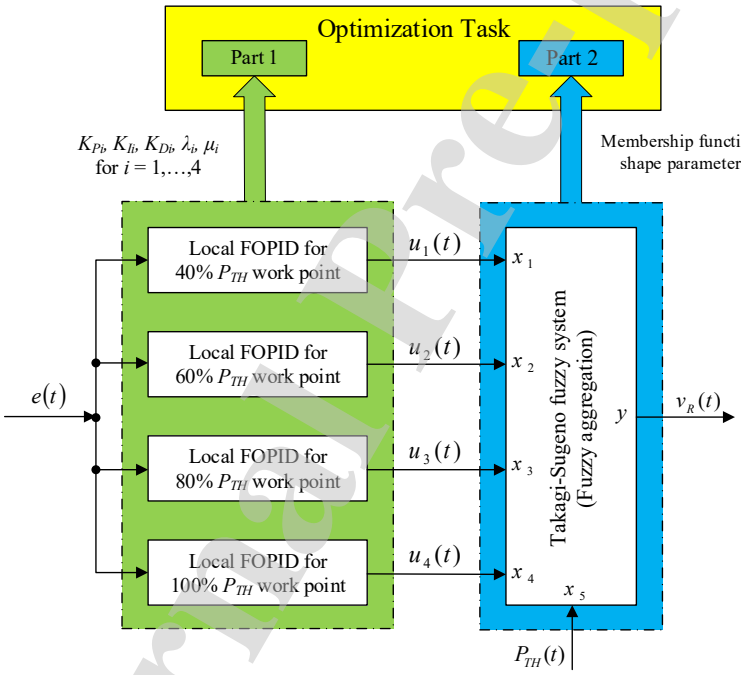

Figure 7 Overview of the multi-regional controller optimization task

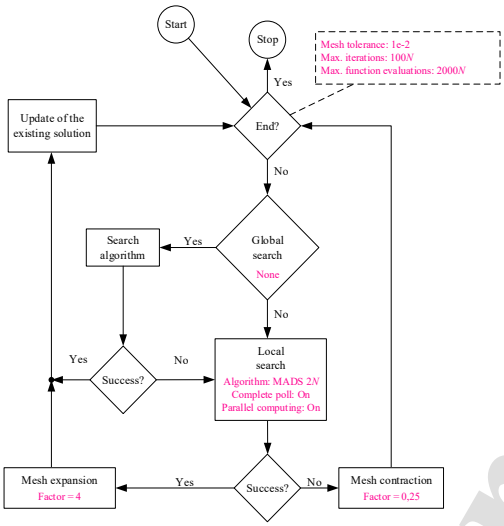

Figure 8 Diagram of the MADS algorithm with specified parameters used in the first and second part of optimization task

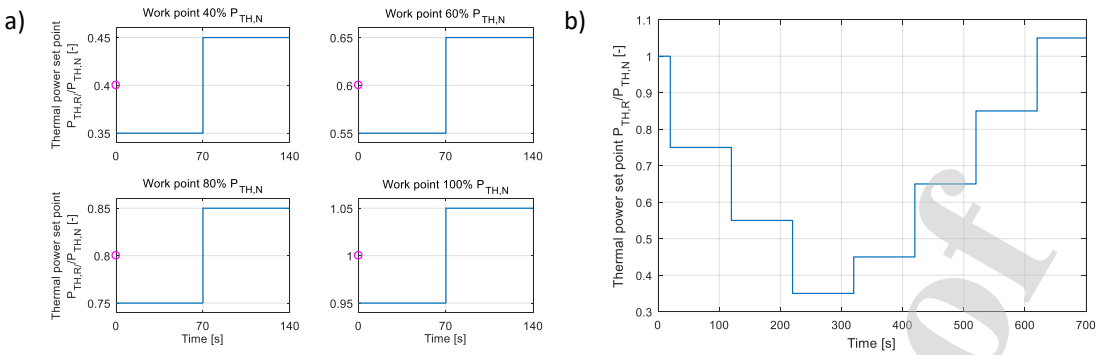

Figure 9 Trajectories of the thermal power set point used in a) first b) second part of optimization task

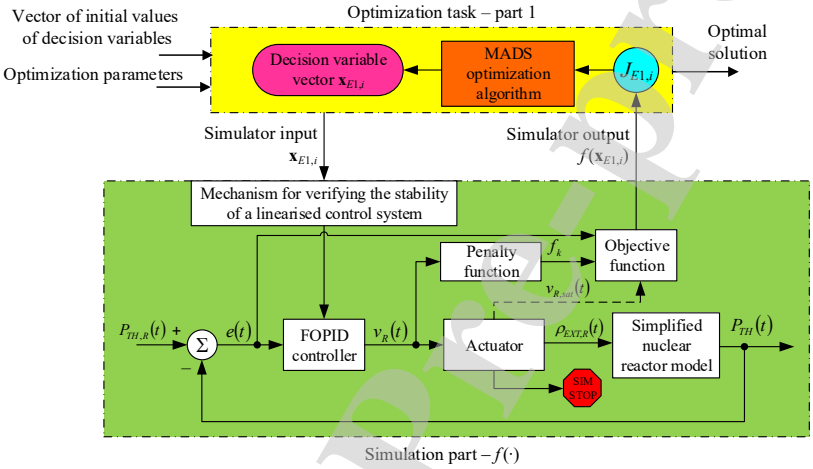

Figure 10 Diagram of the first part of optimization task

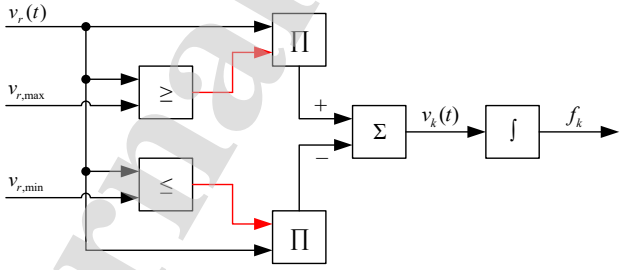

Figure 11 Block diagram of the penalty function: Boolean signals marked red

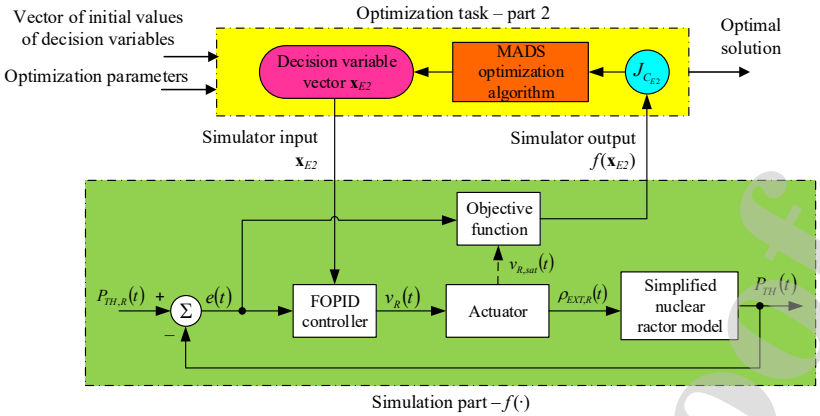

Figure 12 Diagram of the second part of the optimization task

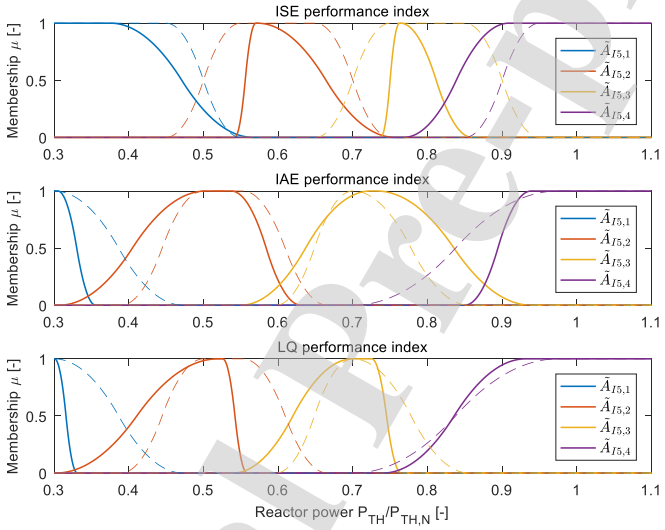

Figure 13 Optimized membership function shapes for the second part of optimization, dashed lines represent function shapes associated with the initial condition of optimization

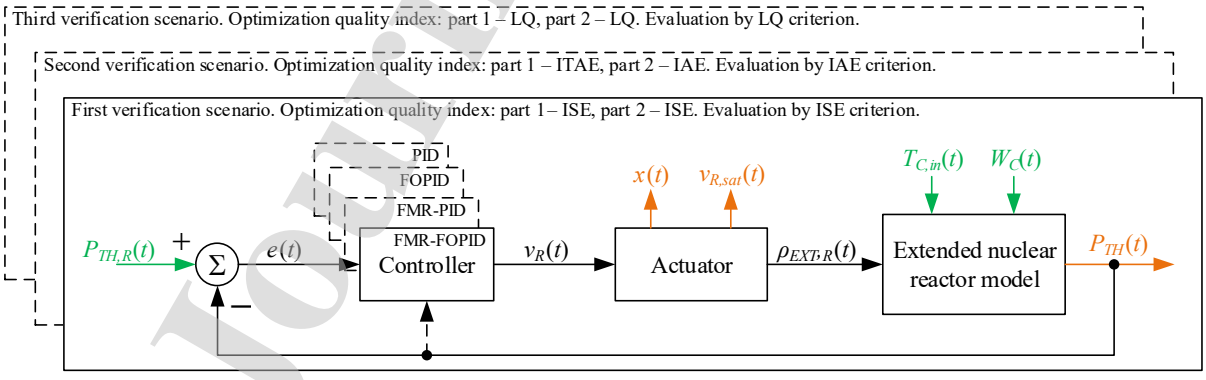

Figure 14 Nuclear reactor thermal power control system used for verification, comparison and robust check purposes, with highlighted scenarios.

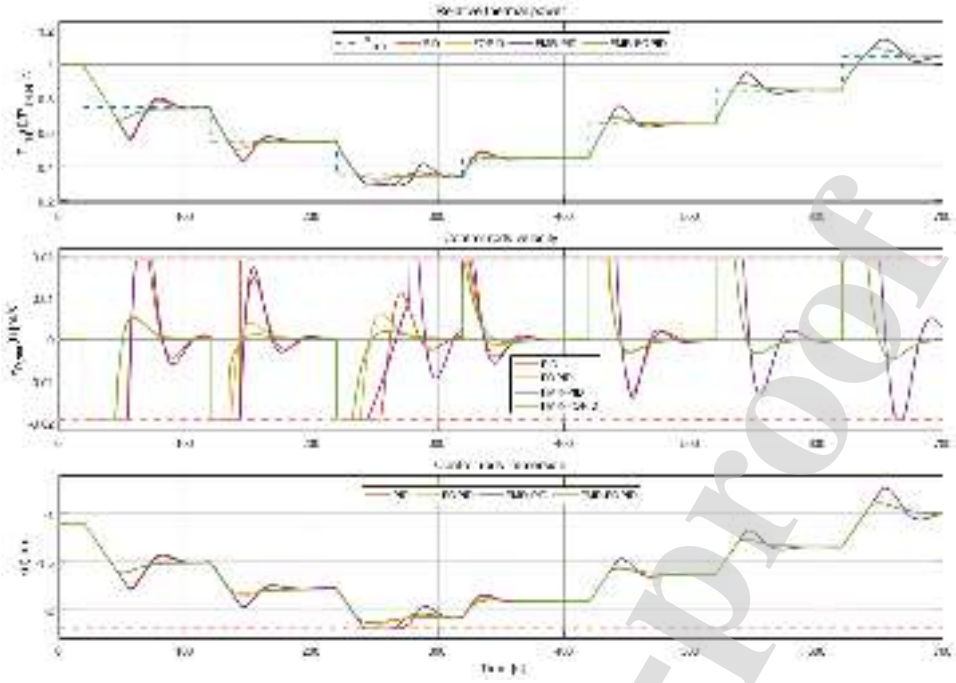

Figure 15 Response of the control system to stepwise trajectory – ISE criterion

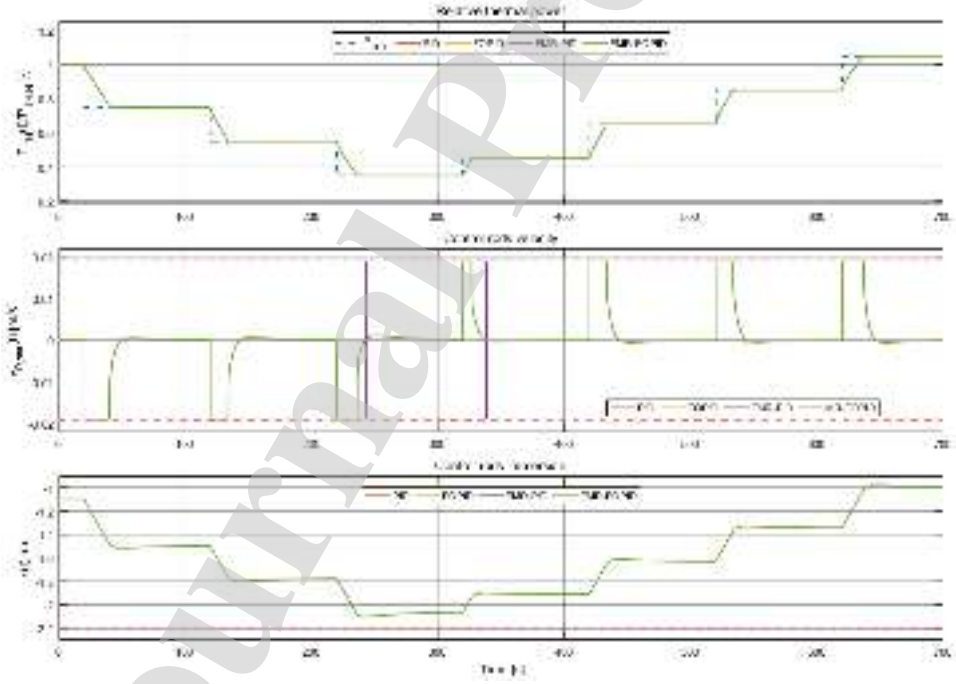

Figure 16 Response of the control system to stepwise trajectory – IAE criterion

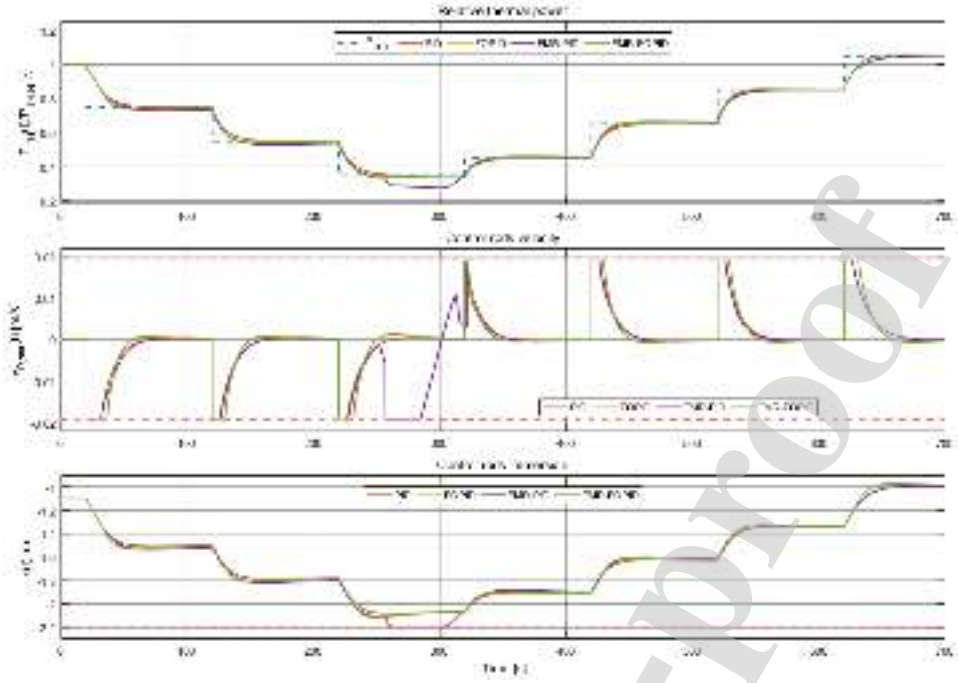

Figure 17 Response of the control system to stepwise trajectory – LQ criterion

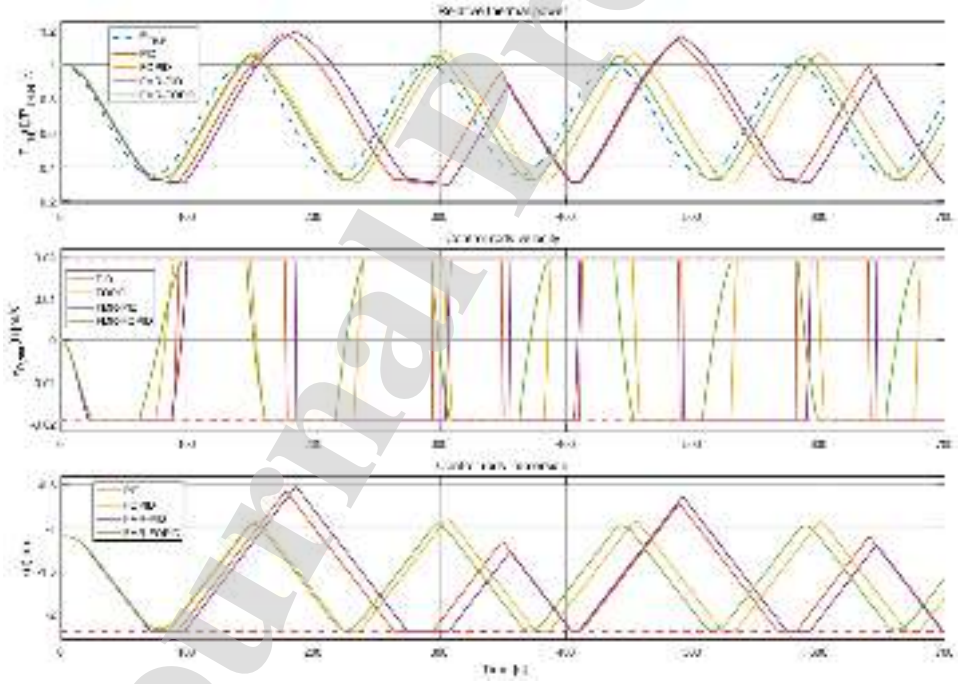

Figure 18 Response of the control system to sinusoidal trajectory – ISE criterion

Figure 19 Response of the control system to sinusoidal trajectory – IAE criterion

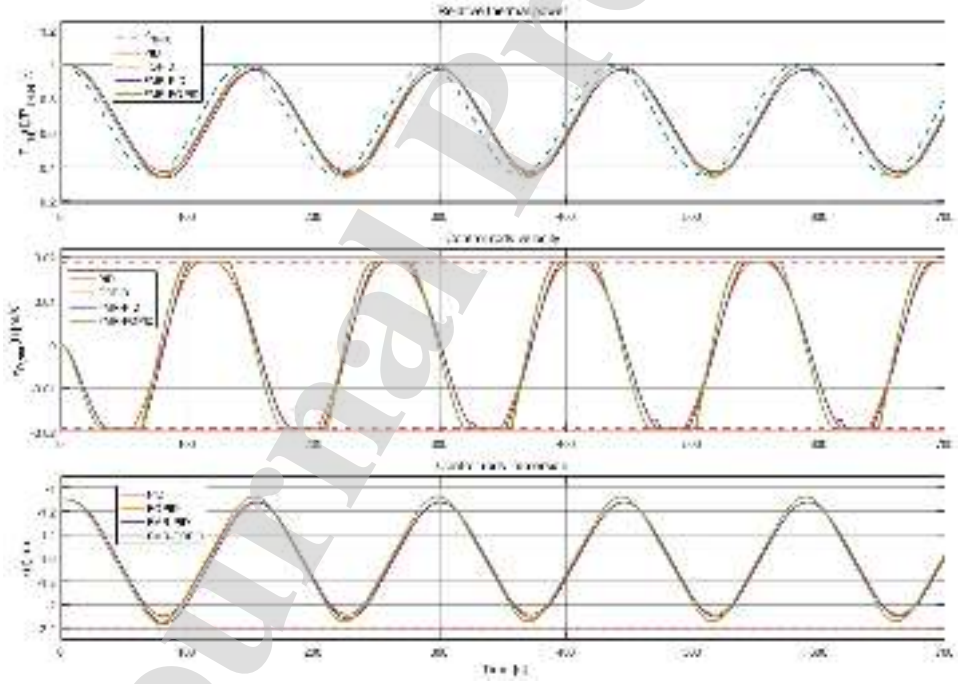

Figure 20 Response of the control system to sinusoidal trajectory – LQ criterion

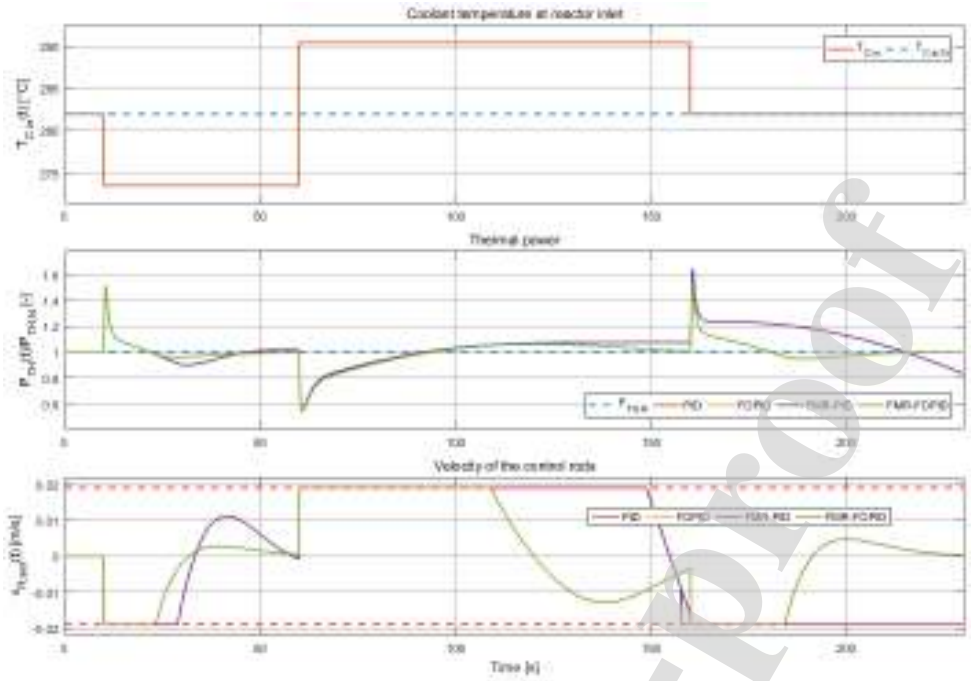

Figure 21. Response of the control system to stepwise coolant temperature changes – ISE criterion.

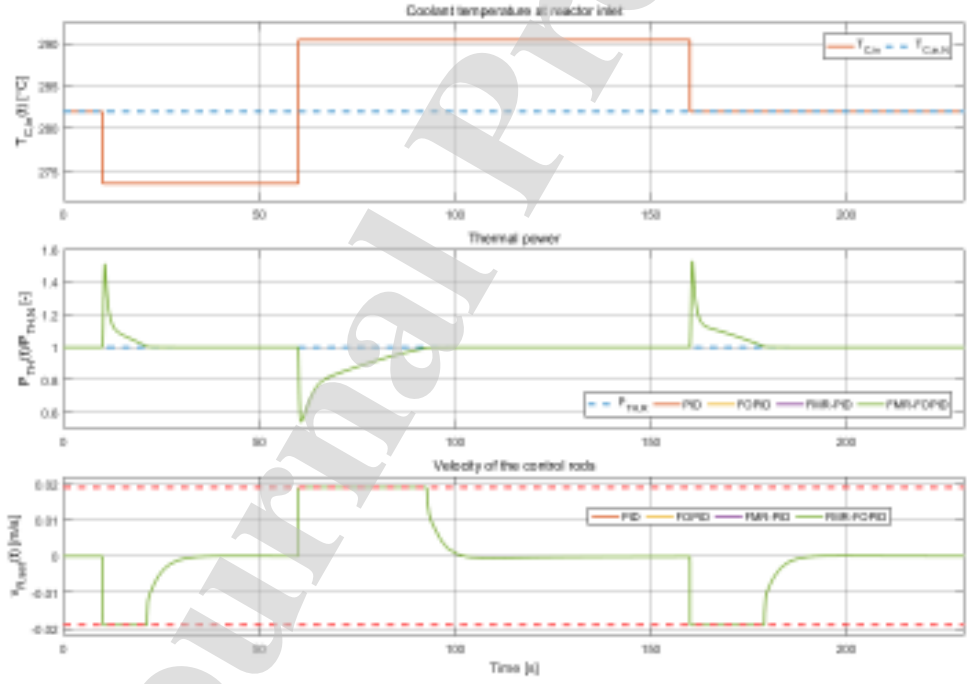

Figure 22. Response of the control system to stepwise coolant temperature changes – IAE criterion.

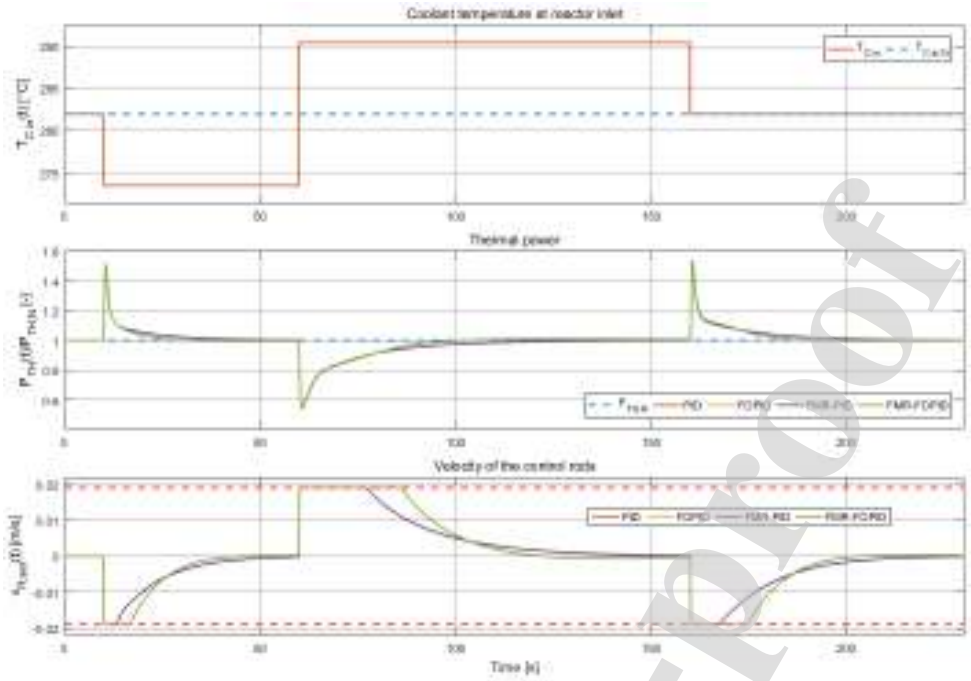

Figure 23. Response of the control system to stepwise coolant temperature changes – LQ criterion.

Appendix A

Table A.1 Parameters of nuclear reactor core models. Nominal parameters for 100% power output are marked with index N.

β	-	0.006502	Λ	s	17.9×10^{-6}	m_F	kg	101032.7109
β_1	-	0.000215	λ_1	1/s	0.0124	m_C	kg	11196.2019
β_2	-	0.001424	λ_2	1/s	0.0305	c_{pF}	J/(kg °C)	247.0212
β_3	-	0.001274	λ_3	1/s	0.1110	c_{pC}	J/(kg °C)	5819.6520
β_4	-	0.002568	λ_4	1/s	0.3010	f_f	-	0.974
β_5	-	0.000748	λ_5	1/s	1.1400	A	m2	5564.8921
β_6	-	0.000273	λ_6	1/s	3.0100	h	W/(m2 °C)	1135.6527
α_F	1/°C	-1.98×10^{-5}	α_C	1/°C	-3.6×10^{-4}	$N_{0,N}$	n/cm3	2.4995×10^{8}
$P_{TH,N}$	MW	3436	$W_{C,N}$	kg/s	19851.9236	$T_{C,in,N}$	°C	281.9444
ρ_b	Δk/k	0.02334	$\tilde{H}$	m	3.66			

Table A.2 Initial temperature conditions at fuel nodes for extended model of nuclear reactor (5F/10C)

$T_{C1,N}$	°C	283.8606	$T_{C6,N}$	°C	305.2041	$T_{F1,N}$	°C	625.0456
$T_{C2,N}$	°C	285.7768	$T_{C7,N}$	°C	307.8684	$T_{F2,N}$	°C	1130.5780
$T_{C3,N}$	°C	290.4949	$T_{C8,N}$	°C	310.5328	$T_{F3,N}$	°C	1189.7028
$T_{C4,N}$	°C	295.2130	$T_{C9,N}$	°C	311.1090	$T_{F4,N}$	°C	782.2639
$T_{C5,N}$	°C	300.2085	$T_{C10,N}$	°C	311.6853	$T_{F5,N}$	°C	413.7187

Table A.3 States of the simplified nuclear reactor model (1F/2C) at selected work points

	Operation points			
	100%	80%	60%	40%
$T_{C,in}$	281.9444			
W_C	19851.9236			
x	-1.0980	-1.4708	-1.7769	-2.0755
$\rho_{EXT,R}$	0	-0.0037619	-0.0075239	-0.011286
$\bar{n}$	$2.4995\cdot10^{8}$	$1.9996\cdot10^{8}$	$1.4997\cdot10^{8}$	$9.9981\cdot10^{7}$
C_1	$2.4212\cdot10^{11}$	$1.9369\cdot10^{11}$	$1.4527\cdot10^{11}$	$9.6846\cdot10^{10}$
C_2	$6.5195\cdot10^{11}$	$5.2156\cdot10^{11}$	$3.9117\cdot10^{11}$	$2.6078\cdot10^{11}$
C_3	$1.6027\cdot10^{11}$	$1.2822\cdot10^{11}$	$9.6162\cdot10^{10}$	$6.4108\cdot10^{10}$
C_4	$1.1913\cdot10^{11}$	$9.5307\cdot10^{10}$	$7.148\cdot10^{10}$	$4.7653\cdot10^{10}$
C_5	$9.1622\cdot10^{9}$	$7.3298\cdot10^{9}$	$5.4973\cdot10^{9}$	$3.6649\cdot10^{9}$
C_6	$1.2665\cdot10^{9}$	$1.0132\cdot10^{9}$	$7.5989\cdot10^{8}$	$5.066\cdot10^{8}$
T_F	826.3684	717.4836	608.5988	499.7140
T_{C1}	296.8149	293.8408	290.8667	287.8926
T_{C2}	311.6853	305.7371	299.7890	293.8408
$\bar{n}/N_N$	1	0.8	0.6	0.4

Table A.4 D_{Ci} coefficients calculated for $n = 5$ fuel nodes.

	1	2	3	4	5	6	7
Control rod immersion [m]	0,0000	0,3660	0,7320	1,0980	1,4640	1,8300	2,1960
Control rod immersion [%]	0	10	20	30	40	50	60
D_{C1}	0,0955	0,0981	0,1094	0,1290	0,1567	0,1933	0,2361
D_{C2}	0,2500	0,2556	0,2794	0,3175	0,3642	0,4110	0,4345
D_{C3}	0,3090	0,3127	0,3251	0,3352	0,3258	0,2810	0,2261
D_{C4}	0,2500	0,2468	0,2261	0,1794	0,1262	0,0934	0,0826
D_{C5}	0,0955	0,0868	0,0599	0,0389	0,0270	0,0213	0,0207

Highlights:

- synthesis methodology for fractional order fuzzy controller for nuclear reactor
- two stage tuning method based on optimization technique for fuzzy controller
- comparison of the fuzzy controller with classical controller equivalents
- use of the direct search optimisation algorithm for tuning of the fuzzy controller
- an average thermal power control system of a Pressurized Water Nuclear Reactor